Convex and effective yield surfaces for numerical rigid plastic limit analysis of reinforced concrete structures with in-plane forces

Andersen, M.E.M.; Poulsen, P.N.; Olesen, J.F.; Hoang, L.C.

Published in:
Computational Modelling of Concrete and Concrete Structures

Link to article, DOI:
10.1201/9781003316404-63

Publication date:
2022

Document Version
Publisher's PDF, also known as Version of record

Computational Modelling of Concrete and Concrete Structures – Meschke, Pichler & Rots (Eds)

Convex and effective yield surfaces for numerical rigid plastic limit analysis of reinforced concrete structures with in-plane forces

M.E.M. Andersen
Department of Bridges International, COWI A/S, Kongens Lyngby, Denmark

P.N. Poulsen, J.F. Olesen & L.C. Hoang
Department of Civil Engineering, The Technical University of Denmark, Kongens Lyngby, Denmark

ABSTRACT: Many reinforced concrete structures are validated in the ultimate limit state (ULS) using analysis methods based on the theorems of plasticity and the rigid-plastic material model. The rigid-plastic material model significantly simplifies the actual stress-strain relationship of reinforced concrete. However, good agreement with capacities found from experiments has been shown when a reduced or so-called effective concrete compressive strength is used. The effective strength is mainly dependent on the transverse tensile strain when a single material point is considered, and well-accepted expressions are given in the codes. The Modified Mohr-Coulomb yield criterion with an effective strength is combined with the elasto-plastic behavior of the reinforcement to create an effective yield surface for reinforced concrete for plane stress states. Based on this, the paper presents an approximate convex effective yield surface, which can be used for Finite Element Limit Analysis (FELA) calculations. The convex effective yield surface is based on auxiliary strains linked to the reinforcement stresses on a material point level. The effective yield surface is tested on a material point level using an experimental database for reinforced concrete panels and on a structural level with an example of a reinforced concrete deep beam with holes. Both tests yield satisfactory results.

1 INTRODUCTION

Concrete is a material with a highly non-linear material behavior in both compression and tension. Advanced Non-Linear Finite Element Analysis (NLFEA) programs such as Diana (Ferreira 2020), and Atena (Červenka & Červenka 2017) can account for the non-linearity using expressions from, for instance, the fib Model Code (fib 2013). By using these non-linear expressions, detailed modeling of structures is possible. However, the analysis can also be cumbersome and requires expert knowledge to alleviate convergence problems in the loading of the structures. Furthermore, many material parameters are needed to describe the non-linear relationship, which can be challenging to determine.

For these reasons, many designs are validated in the ultimate limit state (ULS) using limit analysis methods based on the theorems of plasticity and the rigid-plastic material model (Drucker, Prager, & Greenberg 1952; Gvozdev 1960). Finite Element Limit Analysis (FELA) applies the theorems of plasticity and is a numerical method based on optimization, and since the problem can be posed as a convex problem, it can be solved efficiently (Anderheggen & Knöpfel 1972).

In a FELA framework based on the lower bound theorem, the structure is divided into stress-based finite elements. Scalable load is applied to the structure, and equilibrium is ensured in elements and on boundaries, while a yield surface constrains the stress state of the elements. The largest possible load which the structure can sustain is then sought. For reinforced concrete, the yield surface is often based on the Modified Mohr-Coulomb yield criterion with the possible inclusion of smeared reinforcement using additional linear constraints.

Using a rigid-plastic material model is an extreme simplification compared to the actual stress-strain relationship. However, in combination with a reduced concrete compressive strength, the load-bearing capacities obtained using these methods have shown good agreement with those obtained from experiments on beams, plates, and other structural elements. The reduced concrete compressive strength is obtained by multiplying the cylinder compression strength with a so-called effectiveness factor, ν. Historically, the effectiveness factor has been obtained empirically for individual problem types, such as beams in bending and beams in shear, through the fitting of experimental results with results from exact rigid plastic solutions. Large test databases exist to make these fits for many

DOI 10.1201/9781003316404-63

different structure types. However, all situations cannot be tested, and a general method is needed. For FELA this would mean the development of an effective yield surface, which is the topic of this paper. Previously the topic has been treated in a purely stress-based approach (Herfelt, Poulsen, & Hoang 2018).

To determine how an effective yield surface would look a deformation-based model is considered since several authors have suggested that the effective compressive strength of concrete is linked to the transverse tensile strain ε_1 (Collins & Vecchio 1982; Hoang, Jacobsen, & Larsen 2012). Expressions to determine the effectiveness factor based on ε_1 exist in, for example, the fib model code. Using these expressions combined with a linear elastic perfectly plastic constitutive law for concrete and reinforcement, the stress state for a given strain state can be found. By repeating this calculation for many different strain states, effective yield surfaces are found in the stress space, depending on the degree of allowed strain. The effective elasto-plastic yield surfaces found in this manner are clearly reduced compared to yield surfaces where the effective strength of concrete is not considered.

The next step is to develop a yield surface that can be used in FELA, approximating the yield surfaces from the deformation-based model. The effective elasto-plastic yield surfaces are not convex due to the expression for the effectiveness factor. Therefore, linearization is performed. Furthermore, the elasto-plastic yield surfaces require knowledge of the strains. However, strains are not available on a structural level in FELA due to the rigid-plastic material model. This challenge is overcome by introducing strains as an auxiliary variable on a material point level. The auxiliary strains are constrained and linked to the stresses of the reinforcement by assuming an elasto-plastic behavior. In this way, an effective and convex yield surface is established.

The effective rigid-plastic and convex yield surface for plane reinforced concrete is tested in two examples. The first example is of a reinforced concrete panel loaded in shear, with and without biaxial compression or tension, to test the performance of the yield surface on a material point level. The second example is of a reinforced concrete deep beam with holes, this example is made to see the performance of the yield surface on a structural level.

2 FINITE ELEMENT LIMIT ANALYSIS

Finite Element Limit Analysis (FELA) is a combination of the domain discretization of the Finite Element Method and limit analysis based on the extremum principles of plasticity as postulated by Gvozdev (1960), and Drucker, Prager, & Greenberg (1952). The method was first proposed by Anderheggen & Knöpfel (1972). This paper will only give a brief explanation of the method. For further information, refer to, e.g., Andersen, Poulsen, & Olesen (2022).

The FELA method of this paper is based on the lower bound theorem and is posed as a constrained optimization problem in the following way:

$$\begin{aligned} &\text{max.} && \lambda && \text{Load parameter} && (1a)\\ &\text{s.t.} && \mathbf{H}\boldsymbol{\beta} = \mathbf{R}_0 + \lambda\mathbf{R} && \text{Stress equilibrium} && (1b)\\ &&& f_i(\boldsymbol{\sigma}_i) \leq 0 && \text{Yield conditions} && (1c) \end{aligned}$$

The parameter λ scales the load, and is maximized via the objective function (1a). Equation (1b) ensures the stress equilibrium between internal and external forces. The stress continuity is ensured by $\mathbf{H}\boldsymbol{\beta}$ where $\mathbf{H}$ is the so-called equilibrium matrix, which consists of contributions from each of the elements, and $\boldsymbol{\beta}$ which is a vector collection of the stress variables. The element used for the calculations is a mixed linear lower bound triangle (Herfelt 2017; Krabbenhøft 2016), which is a relaxed version of the lower bound element by Poulsen & Damkilde (2000). The external forces are given by the constant loads $\mathbf{R}_0$ and scalable loads $\lambda\mathbf{R}$.

The last part of the optimization problem is the yield conditions (1c). The elements have a number of material points which contain stress variables. For a plane model the stress variables will be described by the vector:

$$\boldsymbol{\sigma} = \begin{bmatrix} \sigma_{xx} \\ \sigma_{yy} \\ \sigma_{xy} \end{bmatrix} \tag{2}$$

Equation (1c) states that the stresses of the material points should be on or inside the yield surfaces defined by f_i. These yield surfaces are the subject of this paper.

3 MODELING OF PLANE REINFORCED CONCRETE

The models of this paper all use the so-called *smeared reinforcement* approach, whereby the reinforcement bars are assumed to be placed sufficiently close for this to be a reasonable simplification. Furthermore, the reinforcement is assumed to be orthogonally placed coinciding with the x- and y-axis of the Cartesian coordinate system. The amount of reinforcement is described as the reinforcement ratios $\rho_{s,x}$ and $\rho_{s,y}$, see Figure 1. The yield strength of the reinforcement is f_s and the reinforcement is assumed to carry normal tensile stresses only.

The concrete is assumed to be a material with compressive strength, f_c, and negligible tensile strength. Consequently, the reinforced concrete is considered a composite material, where the compressive capacity comes from the concrete and the tensile capacity from the reinforcement.

The elasto-plastic models also use the modulus of elasticity of concrete and steel, E_c and E_s, as well as the crushing strain of concrete ε_{cu} and the rupture strain of the reinforcement ε_{su}. This paper considers a fixed set of parameters which can be seen in Table 1.

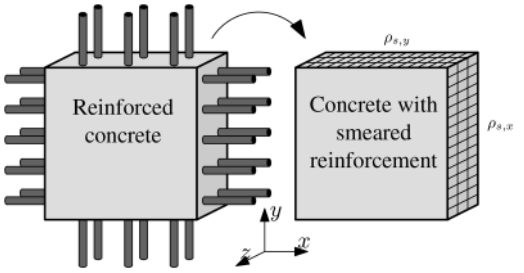

Figure 1. Representative reinforced concrete membrane.

Table 1. Material parameters used to generate the yield surfaces.

f_c	[MPa]	30
E_c	[GPa]	33
ε_{cu}	[‰]	3.5
f_s	[MPa]	500
E_s	[GPa]	210
ε_{su}	[‰]	50
$\rho_{s,x} = \rho_{s,y}$	[%]	0.6

3.1 Separation of stresses

Separation of the total stress into concrete and reinforcement stresses is performed to enable the modeling of the yield surfaces:

$$\boldsymbol{\sigma}_{\square} = \boldsymbol{\sigma}_{\square,c} + \boldsymbol{\rho\sigma}_{\square,s} \tag{3}$$

where $\boldsymbol{\sigma}_{\square}$ is the total stress tensor given by:

$$\boldsymbol{\sigma}_{\square} = \begin{bmatrix} \sigma_{xx} & \sigma_{xy} \\ \sigma_{xy} & \sigma_{yy} \end{bmatrix} \tag{4}$$

and $\boldsymbol{\sigma}_{\square,c}$ is the concrete stress tensor given by:

$$\boldsymbol{\sigma}_{\square,c} = \begin{bmatrix} \sigma_{c,xx} & \sigma_{c,xy} \\ \sigma_{c,xy} & \sigma_{c,yy} \end{bmatrix} \tag{5}$$

and $\boldsymbol{\rho\sigma}_{\square,s}$ is the reinforcement stress tensor given by:

$$\boldsymbol{\rho\sigma}_{\square,s} = \begin{bmatrix} \rho_x & 0 \\ 0 & \rho_y \end{bmatrix} \begin{bmatrix} \sigma_{s,xx} & 0 \\ 0 & \sigma_{s,yy} \end{bmatrix} \tag{6}$$

This separation of stresses is analogue to the way the Nielsen yield criteria is developed (Nielsen & Hoang 2011).

3.2 The effectiveness factor

The effectiveness factor, ν, is a parameter introduced to enable the usage of limit analysis methods based on the theory of rigid-plastic materials for reinforced concrete structures, even though the actual material behavior is not rigid-plastic. However, the limit analysis methods can still be used to provide failure loads in good agreement with tests when a reduction of the concrete compressive strength via the effectiveness factor is applied:

$$f_{c,\text{eff}} = \nu f_c \tag{7}$$

where $f_{c,\text{eff}}$ is the effective concrete compressive strength. The effectiveness factor accounts for several different strength reduction effects related to softening, micro-, and macro-cracking (Nielsen & Hoang 2011). Several authors have suggested formulas for determining the effectiveness factor based on different geometrical and material properties. See Ref. (Hoang, Jacobsen, & Larsen 2012) for an overview of different works. Several of these authors suggest that the effectiveness factor should be a function of the transverse tensile strain, ε_1, and this has also been adopted in the fib model code 2010 (fib 2013) and in the new enquiry version of Eurocode 2 (pr EN1992-1-1 2021). The effectiveness factor for structures that meet the demand for minimum reinforcement may be written in the following way:

$$\nu(\varepsilon_1) = \eta_{f_c}\eta_{\varepsilon}(\varepsilon_1) \tag{8}$$

The first factor, η_{f_c}, accounts for the brittleness of the concrete and can according to (pr EN1992-1-1 2021) be taken as:

$$\eta_{f_c} = \sqrt[3]{f_{c0}/f_c} \leq 1.0, \quad f_c \text{ in MPa} \tag{9}$$

where f_{c0} is a reference strength in the order of 30–40 MPa. In this paper, the value is taken as 30 MPa. The second factor, η_{ε}, is dependent on the transverse tensile strain and can be formulated as:

$$\eta_{\varepsilon}(\varepsilon_1) = \frac{1}{c_1 + c_2\varepsilon_1} \leq c_3 \tag{10}$$

where c_1, c_2, and c_3 are some calibration constants. Herfelt, Poulsen, & Hoang (2018) chose values of $c_1 = 1$, $c_2 = 80$, and $c_3 = 1$, which have also been adopted here.

The left hand side of equation (10) is non-convex and thus also equation (8), making the formula unusable in a convex optimization framework. For his reason, a simple linear relation is adopted in the convex approximations:

$$\eta_{\varepsilon}(\varepsilon_1) = 1 - a\varepsilon_1 \leq 1 \tag{11}$$

where a is the proportionality factor. Figure 2 shows the graph of the left hand side of Expression (10) and the simple linear expression with different values of the a-parameter. The a-parameters in the figure correspond to the slope required to get a reduction similar to Expression (10) for different maximal strains $\varepsilon_{1,\max}$, at a transverse strain corresponding to the yielding strain of the reinforcement.

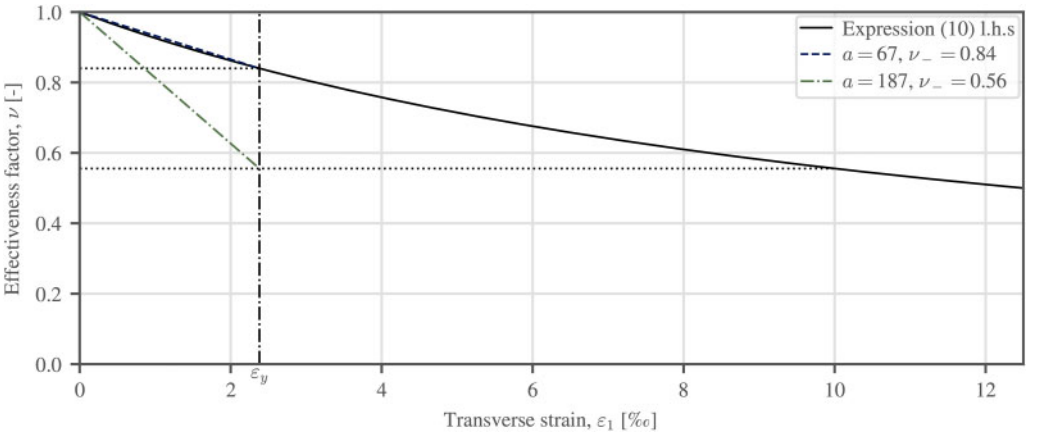

Figure 2. Effectiveness factor as a function of the transverse strain with linear approximations yielding the same reduction at ε_y, as Expression (10) yields for $\varepsilon_{1,\max}$.

4 YIELD SURFACES

Four implementations of yield surfaces for plane reinforced concrete are shown in the following. The yield surfaces are plotted in the $(\sigma_{xx}, \sigma_{yy}, \sigma_{xy})$-coordinate system. Only the positive values of the shear stress are plotted since the yield surfaces are symmetrical with respect to the $(\sigma_{xx}, \sigma_{yy})$-plane.

The rigid-plastic yield surface for plane stress states, is presented as a reference. The rigid-plastic yield surface can only consider a constant reduction of the compressive strength. Therefore, it is a helpful comparison, to see the effect of the reductions due to the transverse strain. Thereafter, two effective elasto-plastic yield surfaces are developed, one as a lower envelope and one as an upper envelope of the effective yield surface. Lastly, a convex effective rigid-plastic yield surface is developed.

4.1 *Rigid-plastic reinforced concrete yield surface*

If only a fixed value of the effectiveness factor is considered, a rigid-plastic yield surface can be developed based only on the concrete compressive strength f_c, the reinforcement yield strength f_s, and the reinforcement ratios $\rho_{s,x}$ and $\rho_{s,y}$.

The Rigid-plastic reinforced concrete yield surface separates stresses into concrete and reinforcement stresses as described above. The concrete should then abide by the Modified Mohr-Coulomb yield criterion with a tensile cutoff of zero and the reinforcement by a simple uni-axial relation. The mathematics of the yield surface is described in Nielsen & Hoang (2011), and a convex implementation can be found, e.g., in Herfelt (2017). A plot of the yield surface can be seen in Figure 3 using the material parameters of Table 1.

It should be noted that Nielsen proposed introducing the effectiveness factor by an additional constraint $|\sigma_{xy}| \leq 0.5\, \nu f_c$ on the shear stress. This additional constraint is omitted for the comparisons in this paper.

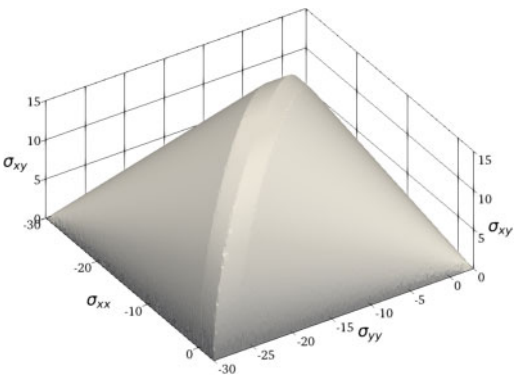

Figure 3. The rigid-plastic reinforced concrete yield for parameters in Table 1.

4.2 *Effective elasto-plastic reinforced concrete yield surface*

The following shows the methodology used to generate two different effective elasto-plastic yield surfaces. These two yield surfaces will represent an upper and a lower bound envelope, of which the significance will be explained later.

The model takes a strain tensor in the form:

$$\boldsymbol{\varepsilon}\square = \begin{bmatrix} \varepsilon_{xx} & \varepsilon_{xy} \\ \varepsilon_{xy} & \varepsilon_{yy} \end{bmatrix} \tag{12}$$

and based on the constitutive equations of the reinforcement and concrete determines a stress state. This process is repeated many times for different strain tensors. The strain tensors are generated in a step-wise process. A unit strain tensor is generated, which is equivalent to a direction in the strain space. The unit strain tensor is then multiplied by a linearly increasing factor to control the magnitude. By repeating this for many different unit strain tensors the strain space is covered. Applying the non-linear constitutive relation will result in many different stress tensors, and

thus a so-called point cloud will be generated in the plane stress space. The two yield surfaces can then be determined from the point cloud by certain criteria.

4.2.1 *Constitutive relation of the reinforcement*

The constitutive relation for the reinforcement is a simple uniaxial relation in each of the two directions, since the reinforcement is assumed only to carry normal stresses and to be placed according to the (x, y)-coordinate system. The linear elastic perfectly plastic material model is applied:

$$\sigma_{s,n}(\varepsilon_n) = \begin{cases} 0, & \varepsilon_n \leq 0 \\ \varepsilon_n E_s, & 0 \leq \varepsilon_n \leq \varepsilon_s \\ f_y, & \varepsilon_s \leq \varepsilon_n \end{cases} \tag{13}$$

where the subscript n denotes either the x- or y-normal. A graph of the relation can be seen in Figure 4.

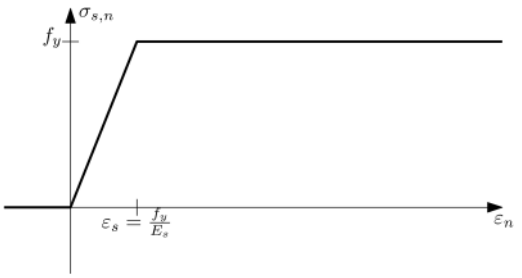

Figure 4. Constitutive relation of the reinforcement.

4.2.2 *Constitutive relation of the concrete*

The constitutive relation of the concrete is based on a linear elastic perfectly plastic relation, same as for the reinforcement. However, the effective uniaxial compressive strength depends on the transverse strain via the effectiveness factor. For these reasons, the constitutive relation of the concrete is based on principal stresses and principal strains. Due to the effect of the transverse strain and the potentially complicated expression for the effectiveness factor, the equations are not easily posed with limits. However, they can be posed in the following way:

$$\sigma_{c,1}(\varepsilon_1, \varepsilon_2) = \min\left\{\max\left\{E_c\varepsilon_1, \nu(\varepsilon_2)f_c\right\}, 0\right\} \tag{14}$$

$$\sigma_{c,2}(\varepsilon_1, \varepsilon_2) = \min\left\{\max\left\{E_c\varepsilon_2, \nu(\varepsilon_1)f_c\right\}, 0\right\} \tag{15}$$

With the usual ordering of the principal strains and stresses, that is, $\varepsilon_1 \geq \varepsilon_2$ and $\sigma_{c,1} \geq \sigma_{c,2}$, only the second principal concrete stress can be influenced by the transverse strain, since if ε_2 is positive ε_1 must also be positive, which implies that $\sigma_{c,1}$ is zero.

A plot of the constitutive relation of the second principal concrete stress as a function of the principal strains can be seen in Figure 5, where material parameters from Table 1 are used. With tensile strain in both principal directions, no concrete stress is present, whereas a linear relation is seen with increasing negative principal strains. The effective compressive strength limits the maximum principal stress, and the increasing transverse strain makes the strength decrease.

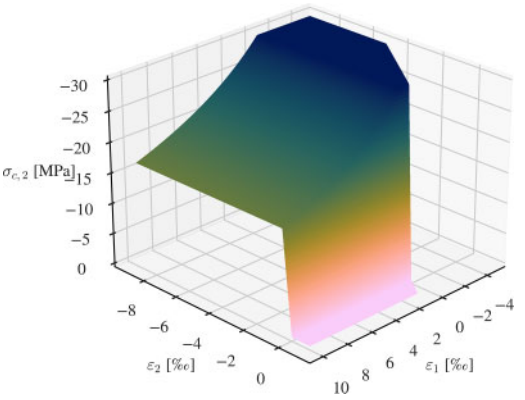

Figure 5. Constitutive relation of the second concrete principal stress in principal strain space.

4.2.3 *Generation of yield surfaces*

With the constitutive relation of the concrete and the reinforcement established, it is possible to determine the corresponding stress state of the composite material for a given strain. The calculation procedure is as follows:

1. Given a strain tensor in the form of equation (12).
2. Compute reinforcement stresses by equation (13) using ε_{xx} and ε_{yy}.
3. Compute principal strains and then compute principal concrete stresses from equations (14) and (15).
4. Transform concrete principal stresses back into directions of original coordinate system.
5. Compute the composite stress state from equation (3).

The above algorithm is used to generate the point cloud of possible stress states from which the yield surfaces are generated. The first yield surface will be called the *upper envelope* (UE) yield surface, which will be generated from the concave envelope of the entire point cloud. The second yield surface will be called the *lower envelope* (LE) yield surface, which will be generated from the concave envelope of the points where there is either no tension and the concrete has reached the crushing strain ε_{cu}, or for points with tension, where the maximum normal tensile strain reaches $\varepsilon_{1,\max} = 10‰$. With these criteria, very similar stress states can exist with varying shear capacity. In these situations, the point with the least shear capacity is shown. The choice of the value 10‰ is arbitrary, and it could be argued that a larger value should be chosen. For instance, the ductility requirement according to the Eurocode for type B reinforcement is required to be 50‰ (Eurocode 2 2008). However, a transverse strain of 50‰ would correspond to a prohibitively

large reduction of the concrete strength, and therefore a lower value is used for these examples.

A plot of the UE yield surface with material parameters from Table 1 can be seen in Figure 6. The coloring on the surface is the perpendicular distance from the current yield surface to the rigid-plastic reinforced concrete yield surface, which can be used to distinguish what has been cut away by introducing the effectiveness factor.

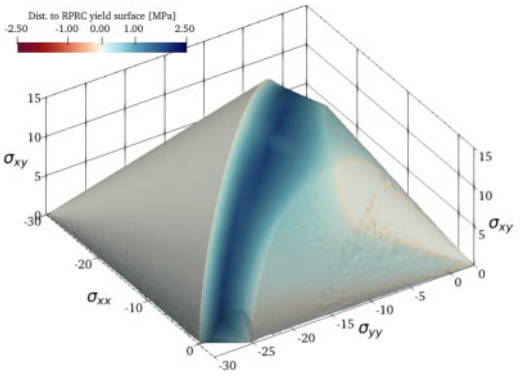

Figure 6. Upper envelope (UE) yield surface.

Firstly, it can be seen that a cone in the compression side of the plot remains unaltered, which is the part corresponding to concrete in biaxial compression. These stresses can be carried without activating the reinforcement in tension, and therefore are not influenced by the effectiveness factor.

Notably, "the right-hand side" of the plot is no longer shaped like a cone. From the coloring of the figure, it can be seen that the reduction is most pronounced in a band around the middle of the yield surface. These are stress states with either predominately shear stress, or shear stress with normal stresses of opposite signs.

From the unaltered part, a decrease in the shear capacity and the maximum compression with transverse tension is seen. Looking at the $\sigma_{xx}\sigma_{yy}$-plane, for maximum transverse tension, it can be seen that the effective compressive strength is reduced from 30 MPa to about 25 MPa. This reduction is equivalent to the effectiveness factor for a transverse strain of ε_y, which is also the required transverse tension to activate the reinforcement fully and thus as expected for the upper envelope.

A plot of the lower envelope yield surface with material parameters from Table 1 can be seen in Figure 7. The cone in the compression part of the yield surface corresponding to biaxial compression is still unaltered. However, the rest of the yield surface is much more reduced due to the larger strains meaning an additionally reduced compressive strength. Looking at the $\sigma_{xx}\sigma_{yy}$-plane, the effective concrete compressive strength is reduced from 30 MPa to about 17 MPa, which is consistent with a transverse strain of $\varepsilon_{1,\max} = 10‰$.

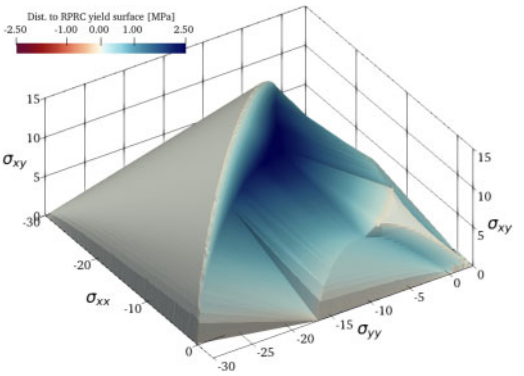

Figure 7. Lower envelope (LE) yield surface.

4.3 *Effective rigid-plastic reinforced concrete yield surface*

To develop a yield surface that can be used in a FELA context, it must be convex and based on the available variables, which are stresses. However, auxiliary strains can be introduced on a material point level by assuming a restriction between the stresses of the model and the auxiliary strains. The strains are introduced as variables: $[\varepsilon_{xx}, \varepsilon_{yy}, \varepsilon_{xy}]$. The strains are linked to the material point and not to a structural deformation-based model, and therefore the strains of the material point are only indirectly influenced by the rest of the structure via the stress equilibrium.

The strains are introduced in relation to the reinforcement stresses in the following way:

$$\sigma_{s,xx} - \varepsilon_{xx} E_s \leq 0 \tag{16a}$$

$$\sigma_{s,yy} - \varepsilon_{yy} E_s \leq 0 \tag{16b}$$

The relations above create a link between the strains and the reinforcement stresses. So in order for the reinforcement to be activated, positive strains are required.

From the plane strains, principal strains can be found in the following way:

$$C_\varepsilon = 1/2(\varepsilon_{xx} + \varepsilon_{yy}) \tag{17a}$$

$$R_\varepsilon = \sqrt{1/2(\varepsilon_{xx} - \varepsilon_{yy})^2 + \varepsilon_{xy}^2} \tag{17b}$$

$$\varepsilon_1 = C_\varepsilon + R_\varepsilon \tag{17c}$$

where ε_1 is the transverse strain. Equation (17b) is equivalent to a second-order cone and can therefore be cast in a convex form. Hereby the transverse strain is available for the implementation.

The concrete stresses should abide by the Modified Mohr-Coulomb yield criterion:

$$\sigma_1 \leq 0 \tag{18a}$$

$$k\sigma_1 - \sigma_3 \leq \nu(\varepsilon_1) f_c \tag{18b}$$

where σ_1, and σ_3 are the largest and smallest principal stress, respectively, and k is the frictional parameter

usually taken as 4. Equation (18a) describes the separation criterion meaning that no concrete tensile strength is considered, and equation (18b) describes the friction criterion. The compressive strength is now a function of the transverse strain via the effectiveness factor. For the proposed yield surface to be convex, the linear approximation of the strain-dependent part of the effectiveness factor, equation (11), is used. The Modified Mohr-Coulomb yield criterion is implemented in the usual manner.

The reinforcement stresses are restricted by simple uni-axial bounds:

$$0 \leq \sigma_{s,xx} \leq f_s \tag{19a}$$

$$0 \leq \sigma_{s,yy} \leq f_s \tag{19b}$$

where f_s is the strength of the reinforcement. With this the effective rigid-plastic reinforced concrete yield surface is presented.

Figure 8 shows the yield surface generated for the material parameters of Table 1 and with the slope parameter a in equation (11) of 67, which is equivalent to a straight line rendering the same value as expression (10) at a transverse strain equal to the yield strain of the reinforcement. The surface is colored after the distance to the UE yield surface shown in Figure 7. The rigid-plastic yield surface generally has the same shape as the UE yield surface, however, as can be seen from the red coloring, the rigid-plastic yield surface is generally less conservative. Figure 9 shows the yield surface with a slope parameter of 187, which is equivalent to a reduction from Expression (10) of 10‰, but at the yielding strain of the reinforcement. This figure is equivalent to the lower envelope and is colored by the distance to the LE yield surface. Again the approximation is quite good. However, there are still areas that are non-conservative with respect to the elasto-plastic yield surface. Nevertheless, this is expected since the non-convex parts can not be accurately captured in a convex approximation.

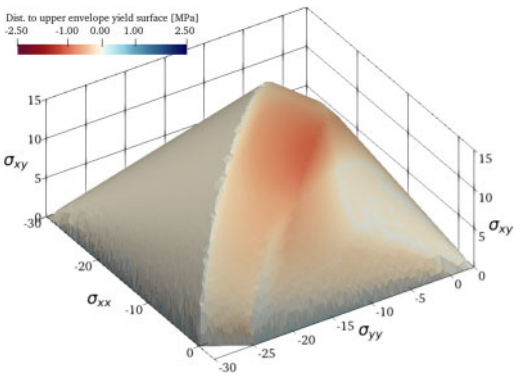

Figure 8. Effective rigid-plastic yield surface with $a = 67$.

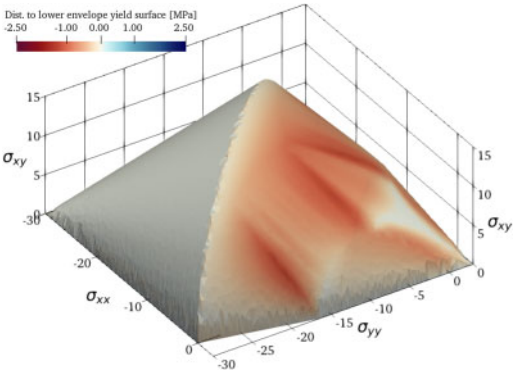

Figure 9. Effective rigid-plastic yield surface with $a = 187$.

5 EXAMPLE: REINFORCED CONCRETE PANEL IN SHEAR WITH AND WITHOUT NORMAL FORCE

The effective yield surface is tested on some experiments of reinforced concrete panels. The reinforced concrete panel experiments have been collected by Hoang, Jacobsen, & Larsen (2012). However, a modified version of the database by Brask & Xuan (2019) is used. The modified database omitted panels that experienced local failure or failure in the experimental setup.

The setup of the panel experiments varies. However, they all seek to emulate a reinforced concrete panel with a concrete stress state in pure shear or shear with biaxial compression or tension. The idealized model in FELA can be seen in Figure 10. The database consists of 72 specimens, with 60 panels in pure shear, 5 in shear with biaxial tension, and 7 with shear and biaxial compression. The biaxial compression and tension are included as a fraction κ of the shear. Of the 72-panels, roughly half ($N = 34$) is isotropically reinforced. The

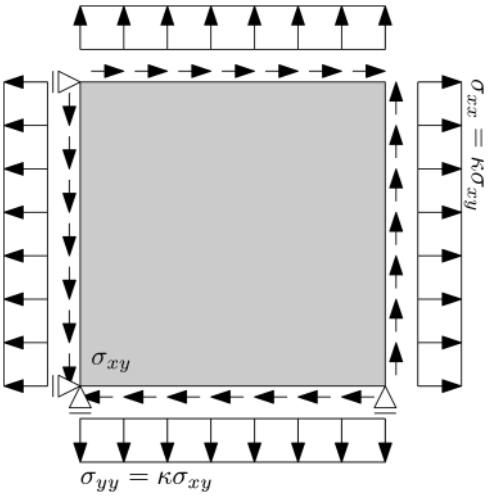

Figure 10. Reinforced concrete panel with shear and normal load.

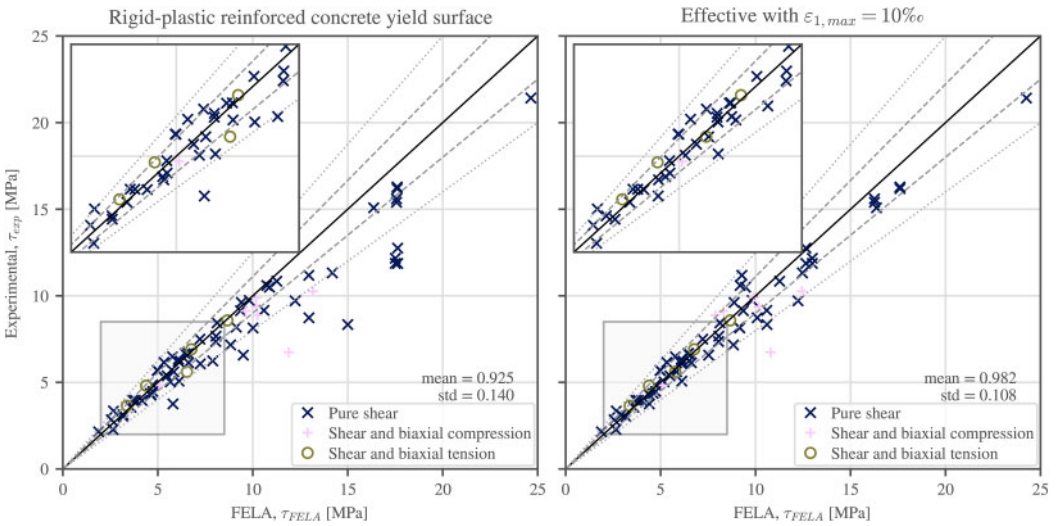

Figure 11. Capacity comparison with reinforced concrete panel experiments.

material parameters for the tests vary, and all the details will not be given here, but they can be found in Brask & Xuan (2019).

The FELA calculations are performed using two yield surfaces. First the rigid-plastic reinforced concrete yield yield surface, where the effectiveness factor is simply 1.0 everywhere (Figure 3), and secondly the effective yield surface with a maximum transverse tensile strain of $\varepsilon_{1,\max} = 10‰$, where the effectiveness factor can vary from 1.0 (Figure 9). The yield surfaces use the material parameters of the specimen and will therefore not be exactly equal to the ones presented so far.

Figure 11 shows a comparison between the experimental capacity τ_{exp} on the ordinate and the capacity found from the FELA calculations τ_{FELA} on the abscissa. The specimens have different markers depending on the loading scenario. The plots also shows a thick line corresponding to $\tau_{\text{exp}} = \tau_{\text{FELA}}$, and two additional lines on either side corresponding to a 5% and 10% deviation. Observations to the right of the thick line will have an overestimated capacity and opposite for points to the left. Furthermore, the plot also shows the basic statistics of the capacity ratio $\tau_{\text{exp}}/\tau_{\text{FELA}}$, where a mean value close to 1 and a low standard deviation would indicate a good fit between the experimental and calculated capacity.

The rigid-plastic reinforced concrete yield generally overestimates the capacity with several data points way outside the 10% deviation line. The result using the effective yield surface is much improved. Almost all the worst outliers are now within the 10% deviation line, and the mean value of the capacity ratio went from 0.925 to 0.982, while the standard deviation has gone down, which indicates that the effective yield surface works well on a material point level. However, one thing to consider is which values of $\varepsilon_{1,\max}$ and the calibration parameters c_1, c_2, and c_3 from equation (10), are used to find the slope parameter a. Since the slope parameter is what defines how much the yield surface is reduced.

6 EXAMPLE: DEEP BEAM WITH HOLES

The previous example showed the behavior of the effective yield surface when compared to experiments performed on reinforced concrete panels. Here the effective yield surface improved the scatter of the results. However, the FELA calculations of those experiments yield a constant stress state over the entire model, and therefore it is also desirable to see the effect on an example with a complicated stress distribution. Therefore, an example for a reinforced concrete deep beam with holes is considered.

A sketch of the beam can be seen in Figure 12. The beam is thicker at the top and the bottom, with the

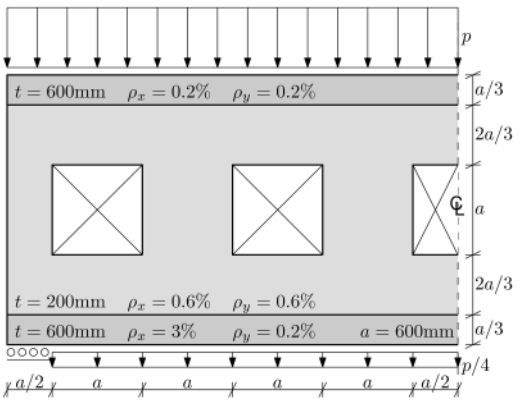

Figure 12. Reinforced concrete deep beam with holes.

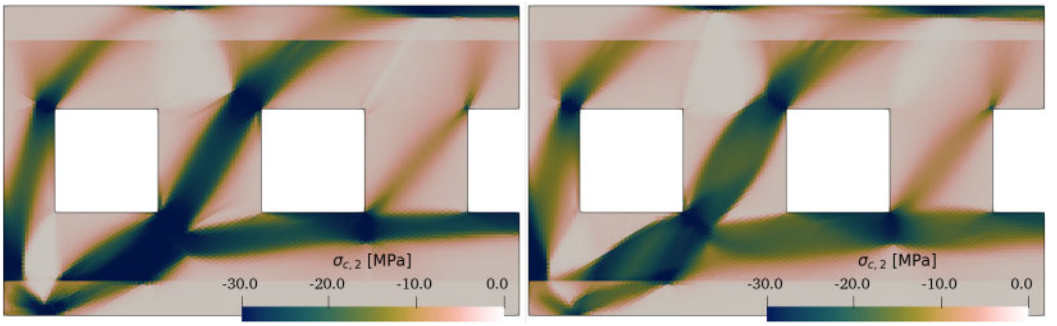

Figure 13. Smallest principal concrete stress for the rigid-plastic reinforced concrete yield surface (left), and the effective yield surface with $a = 187$ (right).

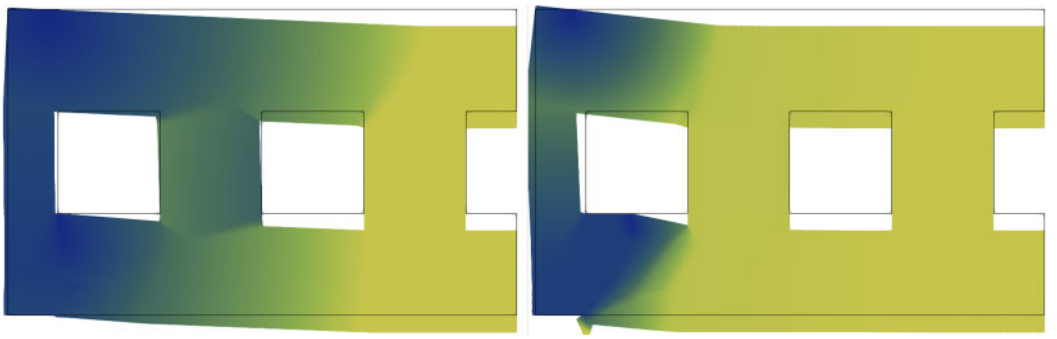

Figure 14. failure mode of the model for the rigid-plastic reinforced concrete yield surface (left), and the effective yield surface with $a = 187$ (right).

top and bottom flanges being three times the thickness of the rest of the beam. The material parameters are the same as listed in Table 1, except for the thickness and the reinforcement ratio. These vary between the web and the flanges. The vertical reinforcement in the flanges is chosen to correspond to the ratio between the thickness of the flanges and the web. Furthermore, horizontal bending reinforcement is added to the bottom flange.

The model is supported vertically at the left end with a support width of 300 mm, and with a symmetry boundary condition on the section at the right-hand side. The loading consists of a distributed load of λp on the top face and $\lambda p/4$ on the bottom face.

For the calculations, an unstructured mesh with an element side length of 25 mm is used, which corresponds to 17160 elements.

The resulting load factor λ is 0.455 using the Rigid-plastic reinforced concrete yield surface and 0.415 using the effective yield surface, which corresponds to $p = 273$ kN/m and $p = 249$ kN/m, respectively. The capacity is thus reduced by 9% when the effective yield surface is used.

Figure 13 shows the value of the smallest principal concrete stress for the model using the rigid-plastic reinforced concrete and effective yield surfaces, respectively. A clear difference between the layout of the compressive stresses is visible. For the rigid-plastic reinforced concrete yield surface, the compression is carried through struts with more or less constant spread and stresses close to f_c, whereas the struts are more diffused in the example with the effective yield surface. This effect is especially visible between the first and the second window when counting from the right, where the strut for the effective yield surface looks like a typical bulging strut, and as such, also has a decreased effective compressive strength.

A comparison of the failure mode using the two different yield surfaces can be seen in Figure 14. The failure mode for the model using the rigid-plastic reinforced concrete yield surface is a combination of a bending and shear failure, whereas the failure mode is much more localized when using the effective yield surface.

7 CONCLUSION

The yield surface of a plane reinforced concrete material point considering the effect of transverse tension on the effective compressive strength has been examined with the goal of developing a convex yield surface for use in Finite Element Limit Analysis (FELA). First, a strain-based elasto-plastic model was developed utilizing an expression for the effectiveness factor similar to the one given in the fib model code. Secondly, a

stress-based convex effective yield surface was developed. The yield surface limits the effective concrete compressive strength by introducing strains linked to the reinforcement stresses on a material point level. The convex yield surface applied a linearized approximation of the effectiveness factor expression. The convex effective yield surface was compared to the elasto-plastic yield surface and was found to be a good approximation. After that, two examples were shown utilizing the effective yield surface compared to the rigid-plastic reinforced concrete yield surface where the effective compressive strength is not considered. The first example used a test database of reinforced concrete panels. The panels were subjected to shear stresses with and without biaxial compression or tension. The effective yield surface improved the predicted failure load compared to the experimental failure load, which indicates that the effective yield surface works well on a material point level. The second example was of a reinforced concrete deep beam with holes. Here the use of the effective yield surface reduced the capacity of the beam by 9%, and a difference in the stress flow and failure mode was seen, which indicates that the effective yield surface also works well on a structural level.

REFERENCES

Anderheggen, E. & H. Knöpfel (1972, dec). Finite element limit analysis using linear programming. *International Journal of Solids and Structures 8*(12), 1413–1431.

Andersen, M. E. M., P. N. Poulsen, & J. F. Olesen (2022, jan). Partially mixed lower bound constant stress tetrahedral element for Finite Element Limit Analysis. *Computers & Structures 258*, 106672.

Brask, S. L. & W. Xuan (2019). *Effective compressive strength and ductility of reinforced concrete panels*. Ph. D. thesis, The Technical University of Denmark (DTU).

Červenka, V. & J. Červenka (2017). *ATENA Program Documentation Part 2-2 User's manual for ATENA 3D*. Cervenka Consulting.

Collins, M. & F. Vecchio (1982). *The Response of Reinforced Concrete to In-plane Shear and Normal Stresses*. University of Toronto, Department of Civil Engineering.

Drucker, D. C., W. Prager, & H. J. Greenberg (1952). Extended limit design theorems for continuous media. *Quarterly of Applied Mathematics 9*(4), 381–389.

Eurocode 2 (2008). *Eurocode 2: Design of concrete structures – Part 1-1: General rules and rules for buildings*. European Committee for Standardization.

Ferreira, D. (2020). *Diana User Manual, Release 10.4*. Delft: DIANA FEA.

fib (2013, oct). *fib Model Code for Concrete Structures 2010*. Weinheim, Germany: Wiley-VCH Verlag GmbH & Co. KGaA.

Gvozdev, A. (1960). The determination of the value of the collapse load for statically indeterminate systems undergoing plastic deformation. *International Journal of Mechanical Sciences 1*(4), 322–335.

Herfelt, M. A. (2017). *Numerical limit analysis of precast concrete structures – A framework for efficient design and analysis*. Ph.d. thesis, Technical University of Denmark (DTU), Kgs. Lyngby.

Herfelt, M. A., P. N. Poulsen, & L. C. Hoang (2018). Closed form adaptive effectiveness factor for numerical models. In *The International Federation for Structural Concrete 5th International fib Congress*.

Hoang, L. C., H. J. Jacobsen, & B. Larsen (2012). Compressive Strength of Reinforced Concrete Disks with Transverse Tension. *Bygningsstatiske Meddelelser (Proceedings of the Danish Society for Structural Science and Engineering) 83*(2-3), 23–61.

Krabbenhøft, K. (2016). Shell finite element. Technical report, Optum Computational Engineering.

Nielsen, M. P. & L. C. Hoang (2011). *Limit Analysis and Concrete Plasticity* (3rd ed.). CRC Press.

Poulsen, P. N. & L. Damkilde (2000, oct). Limit state analysis of reinforced concrete plates subjected to in-plane forces. *International Journal of Solids and Structures 37*(42), 6011–6029.

pr EN1992-1-1 (2021). prEN 1992-1-1 ver. 2021-01 Eurocode 2, Design of concrete structures – Part 1-1: General rules – Rules for buildings, bridges and civil engineering structures.